

## **DEM modeling of the critical-state behavior of a granular material**

X. Huang<sup>1)</sup>, \*C.Y.Kwok<sup>2)</sup>, C. O'Sullivan<sup>3)</sup>, L.G. Tham<sup>4)</sup>

<sup>1), 2), 4)</sup> *Department of Civil Engineering, The University of Hong Kong, Haking Wong Building, Pokfulam Road, HK*

<sup>1), 3)</sup> *Department of Civil and Environmental Engineering, Imperial College London, Skempton Building, London SW7 2AZ, UK*

<sup>1)</sup> [u3001607@hku.hk](mailto:u3001607@hku.hk)

### **ABSTRACT**

The critical-state behavior of a granular material was investigated by performing both drained and undrained (constant volume) triaxial simulations on isotropically-compressed assemblies using the three-dimensional distinct element method (DEM). The particle size distribution used was realistic and the samples were composed of spherical particles. A unique critical state line (CSL) was identified which separates the contractive and dilative states regardless of the initial state or drainage condition. The CSL was curved when plotted on the  $e$ - $\log p'$  plane (where  $e$  is void ratio and  $p'$  is mean effective stress). The particle scale mechanics were explored by considering the distribution of normal contact forces, the coordination number ( $Z$ ) and the deviatoric fabric. It is shown that at the particle-scale, there is a linear relationship between  $Z$  and  $\log p'$  at the critical state. Furthermore, a unique critical-state microstructure can be characterized by considering the product of the coordination number and the deviatoric fabric.

### **1. INTRODUCTION**

The central idea of critical-state soil mechanics (CSSM) is that soils, when sheared to a large strain, will approach an ultimate state at which deformation continues without a change of either the void ratio or the stress state. This ultimate state is called the critical state (Roscoe et al. 1958). When the void ratio is plotted against the mean effective stress at the critical state, a locus of points, typically referred to as the critical state line (CSL), is found. The uniqueness of the CSL of sands in the  $e$ - $\log p'$  plane has been shown in many laboratory tests (Been et al. 1991, Verdugo et al. 1996, Carrera et al. 2011). The critical state concept has been successfully applied to clayey soils, while some contradictory opinions still have to be reconciled regarding the critical-state behavior of sands. According to CSSM, the CSL is unique in the  $e$ - $\log p'$  plane, regardless of the initial soil state and the stress path. However, the CSL of sands in the  $e$ - $\log p'$  plane has also been found by some researchers to be dependent on the initial

soil state (Mooney et al. 1998) and the loading conditions (Finno et al. 1996). Laboratory data have shown that the CSL of sands in the  $e$ - $\log p'$  plane is curved rather than straight (Been et al. 1991, Verdugo et al. 1996, Carrera et al. 2011), and this was attributed to particle breakage or asperity damage (Been et al. 1991). Furthermore, there is still a lack of consensus as to whether the steady state (SS) which was proposed based on undrained triaxial test results is identical to the critical state (CS) that originated from drained triaxial tests. It is interesting to note that Li and Wang

(1998) proposed an alternative way to represent the CSL by plotting  $e$  against  $\left(\frac{p'}{p_a}\right)^\alpha$ ,

where  $\alpha$  is a material parameter that has a value of about 0.6-0.8 for Toyoura sand and  $p_a$  is atmospheric pressure (taken here to be 101.3 kPa).

The distinct element method (DEM) has also been employed to study the critical-state behavior of 2D circular systems (Zhang and Thornton 2005) and 3D spherical systems (Sitharam et al. 2009, Yan et al. 2011, Yimsiri et al. 2011). The critical-state behavior of ellipsoid assemblies has been investigated by Ng (2009). The effect of particle shape, e.g., angularity and roundness, on the critical-state behavior was studied by Maeda et al. (2009). Though most prior DEM studies have agreed that the critical state line is unique and is independent of the initial state, some do not agree with this viewpoint, e.g., Zhao and Evans (2011). A clear micro-mechanical explanation of the critical-state behavior has not yet been described and the aim of the current research is to determine whether there are certain micro-mechanical parameters that can reflect the macro-scale behavior at the critical state.

In this study, both drained and undrained DEM simulations were carried out on unbreakable spherical assemblies with the grading of Toyoura sand. The uniqueness of the CSL in the  $e$ - $\log p'$  plane and the origin of the curvature of the CSL in the  $e$ - $\log p'$  plane are discussed. The coordination number and the anisotropy at the critical state are examined and the micro-mechanical evidence for the critical-state behavior is explored.

## 2. NUMERICAL SIMULATIONS

The DEM simulations in this study were performed using PFC<sup>3D</sup> (Itasca 2009). The simplified Hertz-Mindlin contact model was used and the main input parameters are summarized in Table 1. The particle shear modulus ( $G$ ) and Poisson's ratio ( $\nu$ ) were taken as those of quartz (Simmons and Brace 1965). Gravity was not simulated. Cylindrical assemblies composed of spherical particles following the grading curve of Toyoura sand were created using the radius expansion method. As shown in Fig.1, the grading curve of Toyoura sand was approximated by 4 size intervals within which the particle diameters were uniformly distributed. Particles with a diameter below 0.1156 mm were ignored because of their negligible contribution to the overall particle size distribution. During the radius expansion and isotropic compression stage, the coefficients of friction were varied to create samples with different void ratios at each confining pressure. This technique has been used by several researchers (Gong 2008,

Barreto et al. 2009, Sitharam et al. 2009). The coefficients of friction of all samples were changed to 0.25 before drained or undrained tests were conducted. The position of the cylindrical wall was adjusted continuously to maintain a constant confining pressure in the drained simulation and a constant overall volume in the undrained simulation. The pore water was therefore not explicitly simulated, rather the pore water pressures in the undrained simulations were taken to be the difference between the initial confining pressure  $\sigma_{c0}$  and current pressure  $\sigma'_c$  acting on the cylindrical wall (Sitharam et al. 2009). The details of the numerical experiments are given in Table 2. The test identifiers used in Table 2 and in the subsequent figures are composed of three parts. The first part denotes the packing density as D (dense), M (medium dense) or L (loose); the number in the second part gives the magnitude of initial confining pressure in MPa and the third part shows the drainage condition.

Table1 Input parameters for DEM simulations

|                                |                          |
|--------------------------------|--------------------------|
| Particle density               | 2650 kg/m <sup>3</sup>   |
| Wall stiffness                 | 10 <sup>8</sup> N/m      |
| Contact model                  | Simplified Hertz-Mindlin |
| Particle shear modulus G       | 29 GPa                   |
| Particle Poisson's ratio $\nu$ | 0.12                     |
| Coefficient of friction        | 0.25                     |
| Local damping ratio            | 0.2                      |

Table 2 Details of the numerical experiments

| Test ID  | Initial void ratio $e_0$ | Confining pressure $\sigma_0$ (MPa) | Number of particles | Test type |
|----------|--------------------------|-------------------------------------|---------------------|-----------|
| D1-0.5-U | 0.597                    | 0.5                                 | 6603                | Undrained |
| D2-0.1-U | 0.601                    | 0.1                                 | 6995                | Undrained |
| M1-30-U  | 0.634                    | 30                                  | 6783                | Undrained |
| M2-0.5-D | 0.647                    | 0.5                                 | 6783                | Drained   |
| L-1.0-U  | 0.667                    | 1.0                                 | 6783                | Undrained |

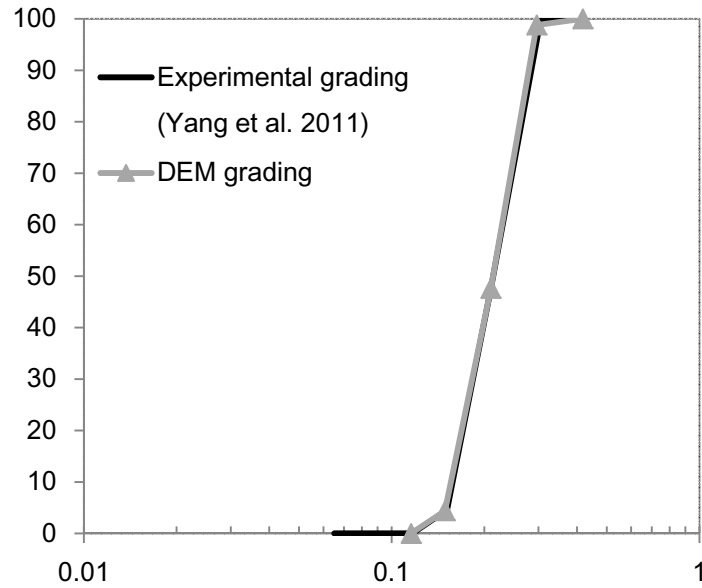


Fig.1 Grading curve of Toyoura sand

### 3. NUMERICAL RESULTS

#### 3.1 Macro-scale results

Fig.2 illustrates the variation of deviatoric stress  $q$  with the axial strain  $\epsilon_a$  in the undrained simulations and Fig.3 shows the corresponding evolution of pore water pressure  $u$ . The dense samples (D1-0.5-U and D2-0.1-U) at a low initial confining pressure exhibited a dilative behavior as indicated by the continuous increase in the deviatoric stress and generation of negative pore water pressure until the steady state was reached. The medium dense sample M1-30-U behaved contractively and only positive pore water pressure was generated throughout the entire simulation. A quasi-steady state at which the deviatoric stress  $q$  reached a local minimum is observed in the loose sample at a medium confining pressure (L-1.0-U). This temporary steady state is followed by an increase in deviatoric stress and an associated decrease in positive pore water pressure. This transition point is called phase transformation point, marking the onset of dilation. As shearing progressed, the deviatoric stress continued to increase and the pore water pressure became negative before the real steady state is approached. The stress-strain behavior of the drained case (M2-0.5-D) is shown in Fig.4. The sample contracted during initial shearing (up to about 0.65% axial strain) but then dilated until the critical state was attained.

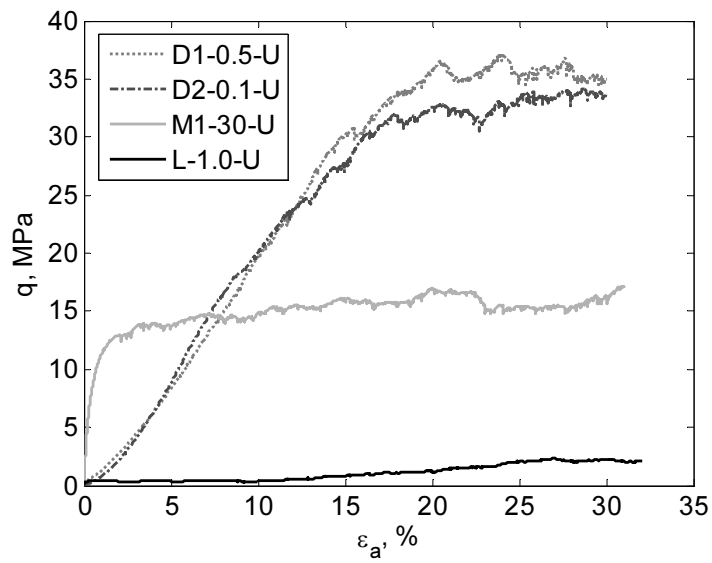


Fig.2 Evolution of deviatoric stress (undrained)

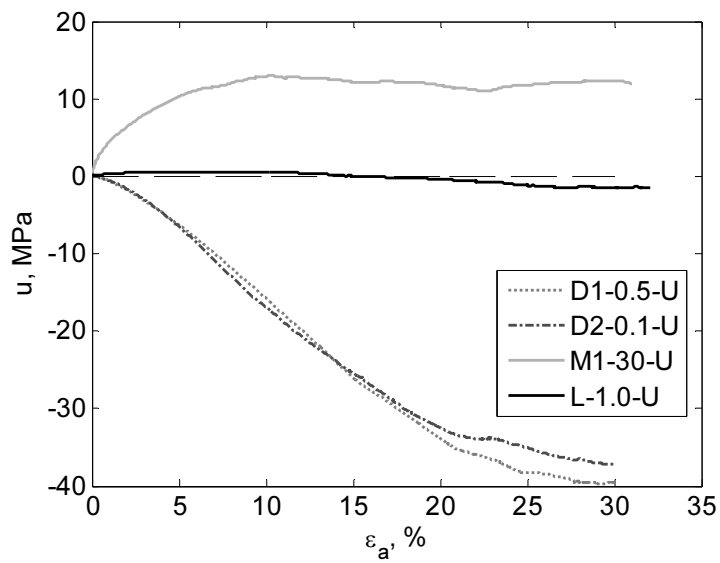


Fig.3 Evolution of pore water pressure (undrained)

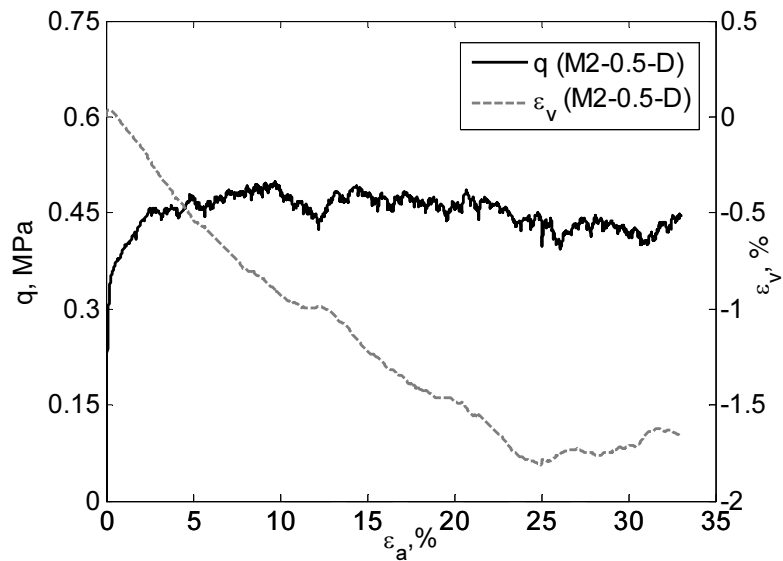


Fig.4 Evolution of deviatoric stress and volumetric strain (drained)

As shown in Fig.5, the stress ratio reached an identical value of 0.64 by about 28% axial strain regardless of the initial state and the drainage condition. The stress paths in the  $q$ - $p'$  plane are shown in Fig.6. It can be observed that all  $(q, p')$  points at 30% axial strain tend to be along the same straight line with a slope  $M$  equalling 0.638, corresponding to a critical state friction angle of  $18^\circ$  calculated from Eq. (1).

$$\phi_{cs} = \sin^{-1}\left(\frac{3 \cdot M}{6 + M}\right) \quad (1)$$

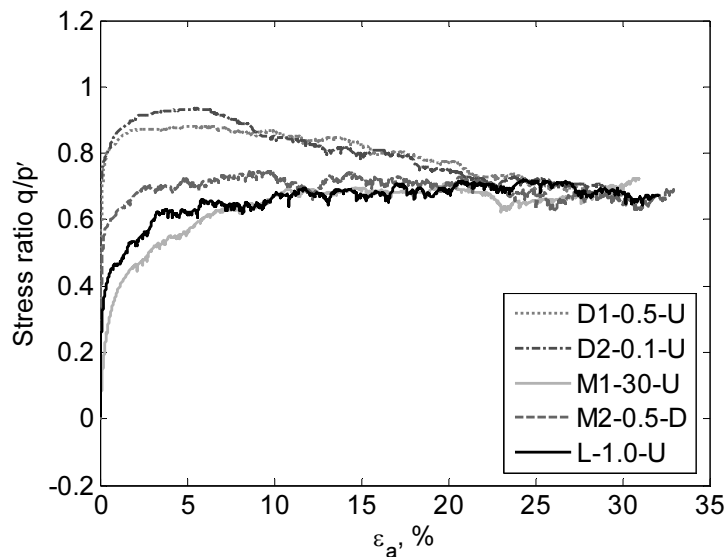


Fig.5 Evolution of stress ratio  $q/p'$

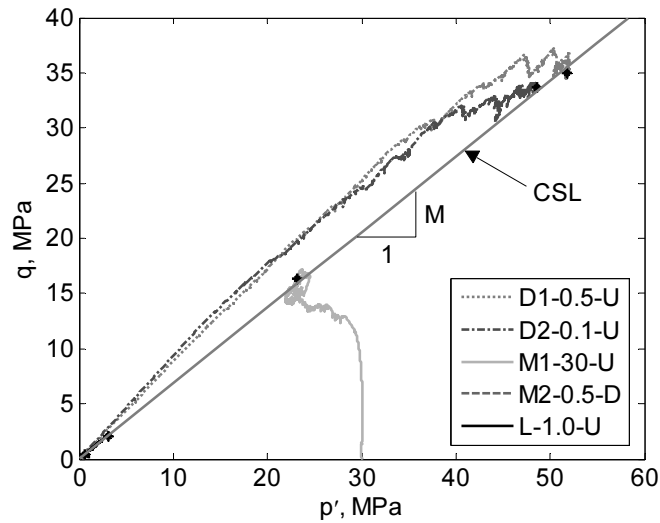


Fig.6 Stress path in the  $p'$ - $q$  plane

Fig.7 and Fig.8 present the critical state points on  $e$ - $\log p'$  plane and  $e$ - $(p'/p_a)^\alpha$  plane respectively, where  $\alpha$  is taken here to be 0.7. The values of  $e$ ,  $q$  and  $p'$  at 30% axial strain are chosen to be the representative ultimate state values in each simulation. It is obvious that regardless of the initial state and drainage condition, a unique critical state line is observed on both the  $e$ - $\log p'$  plane and the  $e$ - $(p'/p_a)^\alpha$  plane. From Fig.7 it is interesting to see that the CSL is still curved in  $e$ - $\log p'$  plane for these non-crushable particles with elastic contacts, indicating that particle breakage and asperity damage may not necessarily explain the curvature of the CSL on  $e$ - $\log p'$  plane. Fig.8 shows clearly that only M1-30-U, which behaves contractively, has an initial state that is above the CSL, while all other samples have initial states that are well below the CSL.

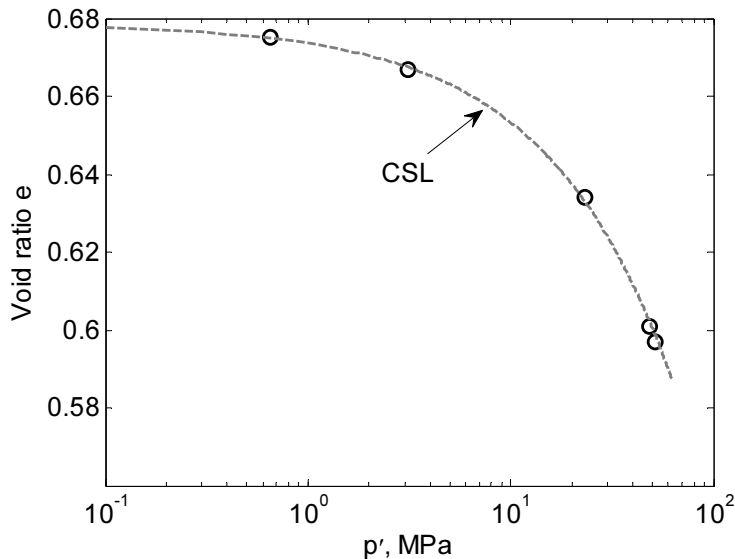


Fig.7 Critical state line on the  $e$ - $\log p'$  plane

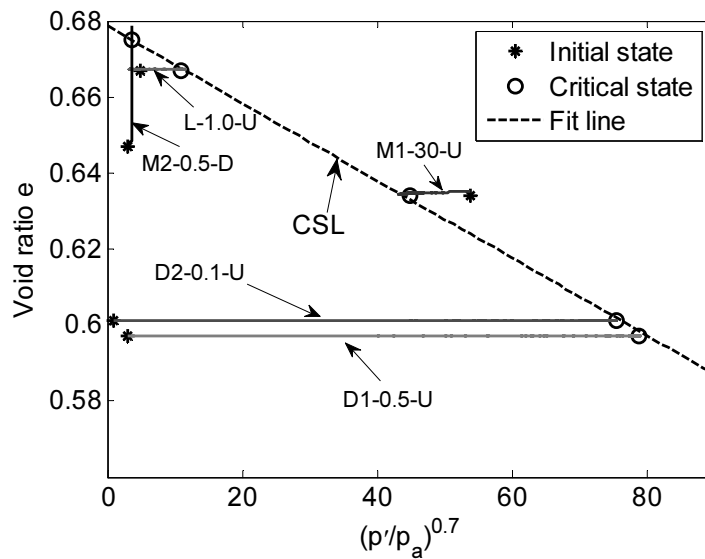


Fig.8 Critical state line on the  $e-(p'/p_a)^\alpha$  plane

### 3.2 Particle-scale results

The coordination number quantifies the average connectivity of particles and has been widely used to evaluate the packing density as well as the structural stability of samples. The conventional definition of coordination number is expressed by Eq.(2).

$$Z = \frac{2 \cdot C}{N} \quad (2)$$

In this equation,  $Z$  is the coordination number, while  $C$  and  $N$  are the numbers of contacts and particles respectively. The evolution of coordination number  $Z$  is presented in Fig.9. The coordination number in the drained case (M2-0.5-D) tends to reach a constant value at a small strain. For the undrained cases (D1-0.5-U and D2-0.1-U), the coordination number increases when the samples begin to dilate and a constant value is attained at large strain levels. However, for the sample without dilation (M1-30-U), the coordination number also reaches a constant value at a very early stage.

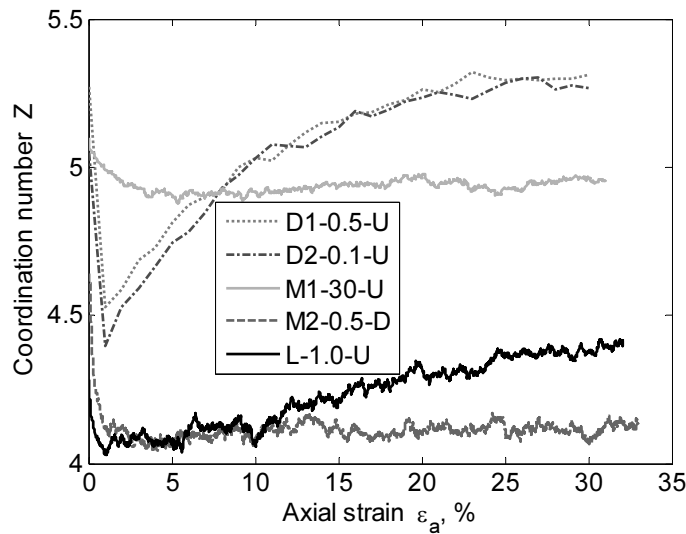


Fig.9 Evolution of coordination number

The coordination number reflects only the contact intensity and gives no information on the contact force magnitude. Several researchers have used probability density functions (PDFs) to study the distribution of contact force magnitudes (Radjai et al. 1996, Antony 2000). The probability density functions of normalized contact normal forces after isotropic compression and at 30% axial strain are shown in Fig.10 (a) and (b) separately. It is worth noting that although the PDF at the initial state depends on both the packing density and stress state, an almost identical PDF is observed at the large strain level despite tiny differences in the distribution of contact forces that are smaller than the average ( $f < 1$ ). As shown in Fig.11, a linear relationship between the mean effective stress and the average contact normal force can be observed. Hence, it may be concluded that the configuration of normal contact force at the critical state is unique irrespective of the initial state and drainage condition.

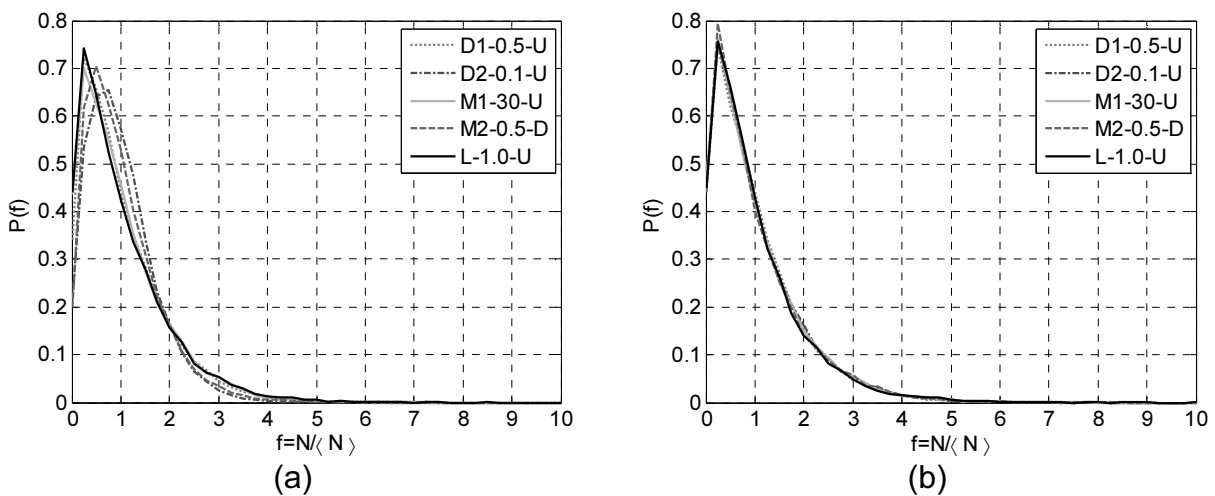


Fig.10 Probability density function of normal contact force

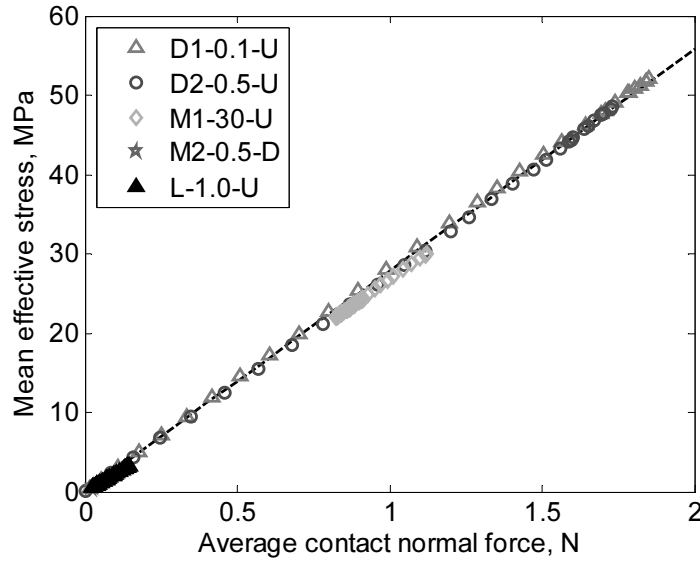


Fig.11 Relationship between the average normal contact force and the mean effective stress

Satake (1982) suggested that the structural anisotropy of a granular assembly composed of disc or sphere particles could be described by the second-order fabric tensor given by Eq.(3).

$$\phi_{ij} = \frac{1}{N_c} \sum_{k=1}^{N_c} n_i^k \cdot n_j^k \quad (i, j = 1, 2, 3) \quad (3)$$

The deviatoric fabric  $\Phi_d$  which is the difference between the maximum eigenvalue  $\Phi_1$  and minimum eigenvalue  $\Phi_3$  of the fabric tensor has been widely used to quantify the structural anisotropy of granular assemblies (Thornton 2000, O'Sullivan et al. 2008). The evolution of deviatoric fabric is illustrated in Fig.12. Prior studies have related the evolution of deviatoric fabric and deviatoric stress (Thornton 2000) or the deviatoric fabric and the principal stress ratio (Maeda 2009, Ng 2009). In the current study comparing Fig.12 with Fig.2 and Fig.4, it is clear that the deviatoric fabric evolves following the same trend of deviatoric stress in the drained case (M2-0.5-D) as well as in the contractive undrained case (M1-30-U). However the evolution of deviatoric fabric in the undrained tests (D1-0.5-U, D2-0.1-U and L-1.0-U) where dilation occurs does not coincide with the evolution of deviatoric stress (Fig.2). Furthermore a unique deviatoric fabric is not observed at large strain levels.

An alternative way to quantify the contact anisotropy is to use the product of coordination number and deviatoric fabric (Maeda 2009, Barreto and O'Sullivan 2012): a parameter termed the deviatoric fabric intensity (Maeda 2009). The physical meaning of this parameter is straightforward as the deviatoric fabric reflects the average anisotropy per contact while the coordination number shows the average connectivity per particle; thus, their product quantifies the contact anisotropy per particle. Fig.13 shows that although the evolution of deviatoric fabric intensity depends on the initial state and drainage condition, an almost identical value of 0.37 is observed at the large

strain levels. This may indicate a real critical state structure. Moreover, it is also interesting to see that the trajectories of the deviatoric fabric intensity are similar to the stress ratio  $q/p'$  against axial strain curves (Fig.5).

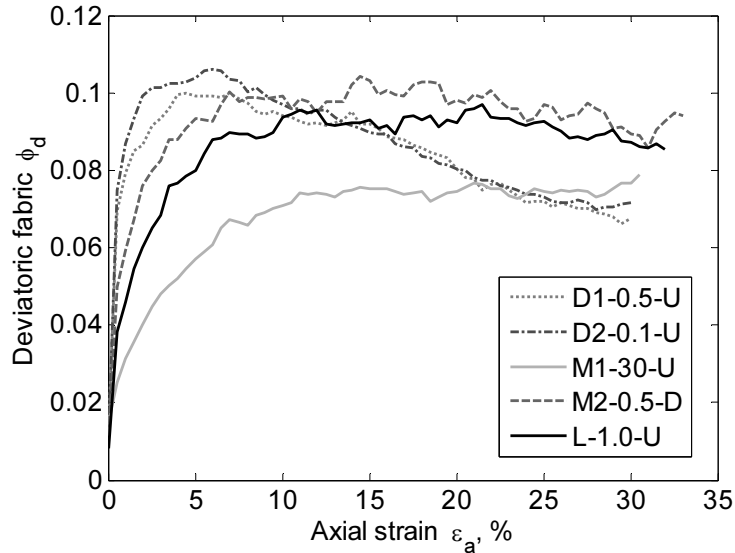


Fig.12 Evolution of deviatoric fabric

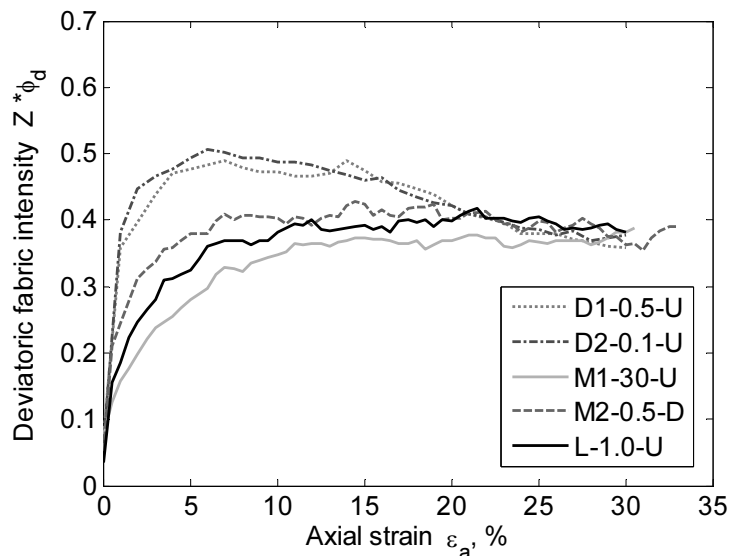


Fig.13 Evolution of deviatoric fabric intensity

As there exists a macro-scale CSL in the  $e$ - $\log p'$  plane, it is natural to anticipate a micro-scale CSL in the  $Z$ - $\log p'$  plane because the coordination number reflects the packing density and is thereby related to the void ratio. The CSL in the  $Z$ - $\log p'$  plane is found to be a straight line as shown in Fig.14, which is in agreement with previous research work (Maeda 2009). It is difficult to anticipate a CSL in the  $\Phi_d$ - $\log p'$  plane as no direct relationship has been found between the deviatoric fabric and the macro parameters. However, since the deviatoric fabric intensity approaches a unique value at the critical state, a relationship can be derived (Eq.4) between the deviatoric fabric and

mean effective stress  $p'$  by considering the linear relationship between  $Z$  and  $\log p'$  at the critical state:

$$\phi_{cri} = \frac{a}{b \cdot \log p' + c} \quad (4)$$

$a$  represents the deviatoric fabric intensity, while  $b$  and  $c$  are the curve fitting parameters of the CSL in the  $Z$ - $\log p'$  plane. The curve predicted by Eq.(4) and the deviatoric fabric obtained in the numerical simulations are plotted together in Fig.15. The predicted curve seems to represent the numerical results quite well.

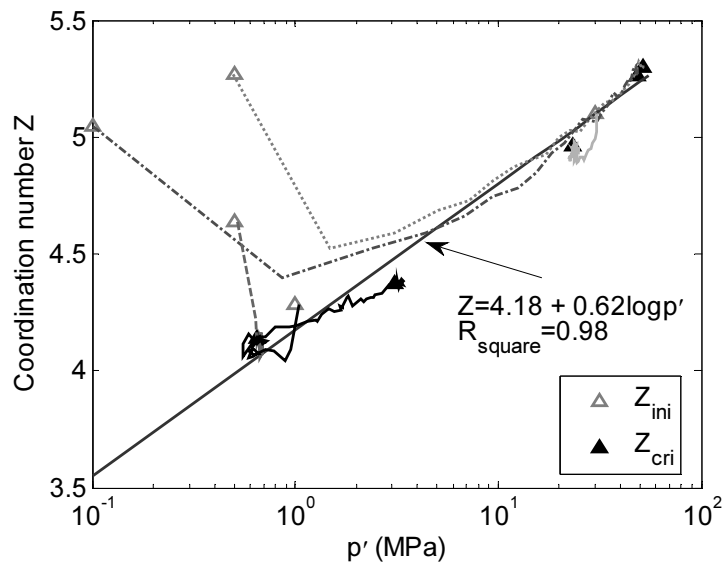


Fig.14 Critical state line in  $Z$ - $\log p'$  plane

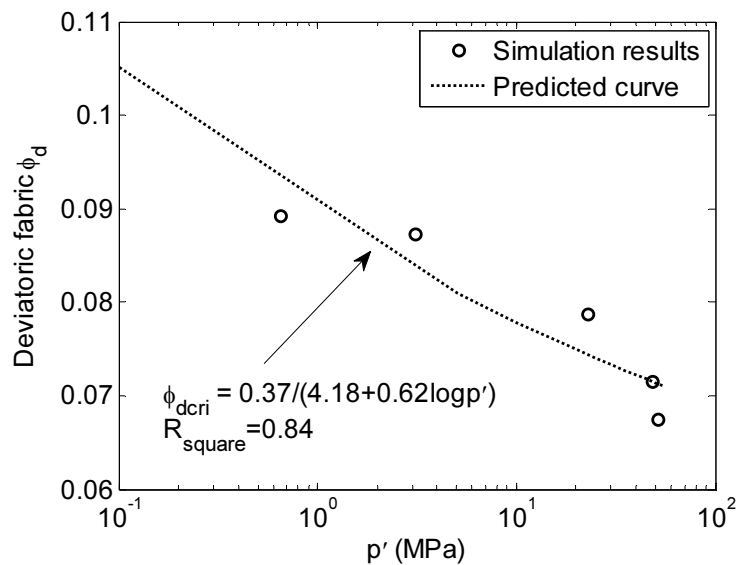


Fig.15 Critical state line in  $\Phi_d$ - $\log p'$  plane

## CONCLUSIONS

This paper has explored the critical state line using DEM simulation results for both drained and undrained triaxial tests. Both macro- and particle-scale behaviors at the critical state have been investigated. The main conclusions can be summarized as follows:

(a) The CSL is unique irrespective of the initial state and drainage conditions;

(b) The curved CSL in  $e$ - $\log p'$  plane is not necessarily due to the change of shearing mechanism resulting from particle breakage or asperity damage as hypothesized by Been et al. (1991);

(c) The unique critical state is characterized by both a unique critical-state microstructure quantified by the deviatoric fabric intensity (the product of the coordination number  $Z$  and the deviatoric fabric  $\Phi_d$ ) and a unique configuration of contact normal force represented by the probability density function of contact normal forces. The difference in the stress magnitude at the critical state may be attributed to the difference in magnitude of the contact forces at the critical state;

(d) The CSL in the  $Z$ - $\log p'$  plane can be well represented by a straight line. Based on this, an expression for the CSL in the  $\Phi_d$ - $\log p'$  plane was derived by considering the unique value of the deviatoric fabric intensity at the critical state.

The conclusions presented here are based on a limited data set and so should be considered as preliminary findings. Additional simulations are required to further develop these ideas.

## REFERENCES

Antony, S.J. (2000), "Evolution of force distribution in three-dimensional granular media", *Phys. Rev. Lett.*, **63**(1), 1-13.

Barreto, D., and O'Sullivan, C. (2012), "The influence of inter-particle friction and the intermediate stress ratio on soil response under generalized stress conditions", *Granul. Matter*, doi: 10.1007/s10035-012-0354-z.

Been, K., and Jefferies, M.G. (1985), "A state parameter for sands", *Géotechnique*, **35**(2), 99-112.

Carrera, A., Coop, M.R. and Lancellotta, R. (2011), "Influence of sample preparation techniques and stress path followed on the location of the critical state line: an example of a silty-sandy tailing", *Proc., 5<sup>th</sup> Int. Symp. on Deformation Characteristics of Geomaterials*, C. K. Chung et al., eds., Seoul, Korea, 526-532.

Finno, R.J., Harris, W.W. and Mooney, M.A. (1996), "Strain localization and undrained steady state of sand", *J. Geotech. Eng., ASCE*, **122**(6), 462-473.

Gong, G. (2008). "DEM simulations of drained and undrained behaviour." Ph.D. thesis, Univ. of Birmingham, UK.

Itasca: PFC-3D: Particle flow code in two dimensions, version 4.0, Minneapolis (2009).

Li, X.S., and Wang, Y. (1998), "Linear representation of steady-state line for sand", *J. Geotech. Geoenviron. Eng., ASCE*, **124**(12), 1215-1217.

Maeda, K., Sakai, H. et al. (2009), "Stress-chain based micromechanics of sand with grain shape effect", *Granul. Matter*, **12**, 499-505.

Mooney, M.A., Finno, R.J. and Viggiani, M.G. (1998), "A unique critical state for sand?", *J. Geotech. Geoenviron. Eng., ASCE*, **124**(11), 1100-1108.

Murthy, T.G., Loulacidis, D. et al. (2007), "Undrained monotonic response of clean and silty sands", *Géotechnique*, **57**(3), 273-288.

Ng, T.T. (2009), "Discrete element method simulations of the critical state of a granular material", *J. Geomech., ASCE*, **9**(5), 209-216.

O'Sullivan, C., Cui, L. and O'Neill, S.C. (2008), "Discrete element analysis of the response of granular materials during cyclic loading", *Soils Found.*, **48**(4), 511-530.

Radjai, F., Jean, M. et al. (1996), "Force distributions in dense two-dimensional granular systems", *Phys. Rev. Lett.*, **77**(2), 274-277.

Roscoe, K.H., Schofield, M.A. and Wroth, C.P. (1958), "On the yielding of soils", *Géotechnique*, **8**(1), 22-53.

Satake, M. (1982), "Fabric tensor in granular materials", *Deformation and failure of granular materials*, P.A. Vermeer and H.J. Luger, eds., Balkema, Rotterdam, The Netherlands, 63-68.

Simmons, G., and Brace, W.F. (1965), "Comparison of static and dynamic measurements of compressibility of rocks", *J. Geophys. Res.*, **70**, 5649-5656.

Sitharam, T.G., and Vinod, J.S. (2009), "Critical state behavior of granular materials from isotropic and rebounded paths: DEM simulations", *Granul. Matter*, **11**, 33-42.

Thornton, C. (2000), "Numerical simulations of deviatoric shear deformation of granular media", *Géotechnique*, **50**(1), 43-53.

Verdugo, R., and Ishihara, K. (1996), "The steady state of sandy soils", *Soils Found.*, **36**(2), 81-91.

Yan, W.M., and Dong, J.J. (2011), "Effect of particle grading on the response of an idealized granular assemblage", *J. Geomech., ASCE*, **11**(4), 276-285.

Yang, J., and Sze, H.Y. (2011), "Cyclic behavior and resistance of saturated sand under non-symmetrical loading conditions", *Géotechnique*, **61**(1), 59-73.

Zhang, L., and Thornton, C. (2005), "Characteristics of granular media at the critical state", *Proc., Powders and Grains 2005*, R. Garcia-Rojo et al., eds., Taylor & Francis Group, London, 267-270.

Zhao, X.L., and Evans, T.M. (2011), "Numerical analysis of critical state behaviors of granular soils under different loading conditions", *Granul. Matter*, **13**, 751-764.